Analytic expressions for linear optical susceptibilities of conjugated polymers

Thomas Bastholm Lynge* and Thomas Garm Pedersen
Institute of Physics, Aalborg University, Pontoppidanstraede 103, DK-9220, Aalborg East, Denmark
(Received 1 August 2002; published 28 February 2003)

Analytic expressions for the complex long-axis linear optical susceptibility χ_{xx} of parallel, noninteracting *trans*-polyacetylene and poly(*para*-phenylene) chains are obtained in terms of the band gap E_g and the π-band width E_0. The fact that the susceptibility expressions show identical dependence on the parameters E_g and E_0 leads the way to a general expression for the long-axis linear optical susceptibility of conjugated polymers valid for photon energies around the band gap. The susceptibility expressions include damping and are obtained in the free-carrier dipole approximation using an analytic tight-binding derivation based on carbon π electrons only. In addition to the long-axis susceptibilities, the complex short-axis susceptibility χ_{yy} and off-diagonal susceptibility χ_{xy} of *trans*-polyacetylene and the imaginary part of the short-axis susceptibility of poly(*para*-phenylene) are also derived.

DOI: 10.1103/PhysRevB.67.075206 PACS number(s): 78.67.Lt, 42.70.Jk, 72.80.Le, 78.30.Jw

I. INTRODUCTION

Due to the vast technological potentialities of conjugated polymers, a lot of research effort has been invested in this area within the last few decades. One of the pioneering efforts leading to an overall interest in organic materials was the 1963 reporting of electroluminescence from organic semiconductors.[1] Following the 1977 report of metal-sized conductivities in doped polyacetylene,[2] a substantial part of that interest was devoted to conjugated polymers. As for actual applications, polymer light emitting diodes (PLED's) showing attractive device characteristics have now been produced.[3] These PLED's owe their technological success to the following characteristics of conjugated polymers[4]: charge transport ability, high-efficiency electroluminescence in the visible with emission wavelength tunable by chemical modification, and the simple processing techniques common to all plastics. Furthermore, the fast response times characteristic of organic materials in general make the use of conjugated polymers appealing in connection with photodetection.[5]

Being the simplest of all conjugated polymers, the electronic, optical, and structural properties of polyacetylene $[(CH)_x]$ have been thoroughly investigated over the years.[6–16] Since information about optical properties such as index of refraction, absorption, etc., can be derived from the susceptibility tensor $\overleftrightarrow{\chi}$, the derivation of optical properties typically amounts to calculating components of either the susceptibility tensor or the closely related dielectric tensor $\overleftrightarrow{\varepsilon}$. Pioneering the field of calculating the optical properties of conjugated polymers, Cojan *et al.*[6] derived an analytic expression for the long-axis optical susceptibility of polyene chains, such as *trans*-polyacetylene. Later, Baeriswyl *et al.*[9] found an analytic expression for the imaginary part of the dielectric tensor of *trans*-polyacetylene, and Neumann and von Baltz[16] found an analytic expression for the real and imaginary parts of the long-axis dielectric function of *trans*-polyacetylene. In all three cases the treated chains were parallel and infinite, and damping was not included.

As another promising conjugated polymer,[17] which, e.g., was the first polymer used in PLED's showing blue emission at room temperature,[18–20] poly(*para*-phenylene) has also drawn substantial interest over the years.[13,21–23] The obtained results, however, have been less exhaustive than in the case of polyacetylene, and, in particular, no analytic expression for the various susceptibilities associated with poly(*para*-phenylene) has to our knowledge ever been derived. Such analytic expressions would increase the understanding of the optical properties of poly(*para*-phenylene) and might ultimately serve to improve the application of poly(*para*-phenylene), e.g., in connection with PLED, photovoltaic, or photodetecting devices.

The purpose of this paper is first to derive analytic closed-form expressions including damping for the complex linear optical susceptibilities of infinite, parallel *trans*-polyacetylene and poly(*para*-phenylene) chains, respectively. For *trans*-polyacetylene the complete susceptibility tensor is calculated, and for poly(*para*-phenylene) the complex long-axis susceptibility and the imaginary part of the short-axis susceptibility are calculated. Second, the purpose is to obtain through comparison a general expression for the complex long-axis linear optical susceptibility applicable to all conjugated polymers. The inclusion of damping, the calculations for poly(*para*-phenylene), and the comparison of the long-axis susceptibilities of an acetylene- and a phenyl-based polymer make the present results more general than the previous results in this field.[6,9,16]

Throughout this paper, all excitonic and polaronic effects are disregarded. These important extensions will be considered in future work.

II. THEORY

In this paper the conjugated polymers are treated as planar molecules lying in the xy plane. In such conjugated polymers three of the four valence electrons of the carbon atoms form sp^2-hybridized bonds and the fourth electron forms a delocalized π orbital with $2p_z$ symmetry. As the excitation energy is smaller for the π electrons than for the sp^2 electrons, the π electrons will be the main contributors to the low-photon-energy part of the susceptibility. Furthermore, since, due to symmetry, the π orbitals couple to other π orbitals only, the π electrons can be treated seperately.

A. Band structure

The π-band states are characterized by a band number r and a crystal wave number k and are therefore written $|rk\rangle$. In a tight-binding treatment, the π states are expanded in the atomic $2p_z$ orbitals, yielding

$$|rk\rangle = \frac{1}{\sqrt{N}} \sum_{n,p=1,1}^{N,P} r_p(k) e^{iknl} |np\rangle,$$

$$k = \frac{2\pi}{Nl} u, \quad u \in \{0,1,\ldots,N-1\}, \tag{1}$$

where l is the lattice constant, $|np\rangle$ is the $2p_z$ orbital centered at the pth carbon atom in the nth unit cell, N is the number of unit cells, and P is the number of atomic sites in the unit cell. Inserting Eq. (1) into the energy eigenvalue equation

$$\mathcal{H}|rk\rangle = E_r(k)|rk\rangle \tag{2}$$

and applying the atomic orbital $\langle mq|$ from the left yields

$$\sum_{n,p} e^{iknl}[\langle mq|\mathcal{H}|np\rangle - E_r(k)\langle mq|np\rangle] r_p(k) = 0. \tag{3}$$

Equation (2) is thus seen to be equivalent to a $p \times p$ matrix eigenvalue problem. In this paper wave function overlap will be disregarded[26] ($\langle mq|np\rangle = \delta_{mn}\delta_{pq}$) and only Hamilton matrix elements $\langle mq|\mathcal{H}|np\rangle$ between nearest neighbors will be considered.

B. Electric dipole matrix element

The x and y components of the electric dipole matrix element between valence and conduction bands v and c are given by

$$d_{cv}^x = -e\langle ck|x|vk\rangle, \tag{4a}$$

$$d_{cv}^y = -e\langle ck|y|vk\rangle, \tag{4b}$$

where $e>0$ is the elementary charge. As linear combinations of $2p_z$ orbitals all valence- and conduction-band states $|vk\rangle$ and $|ck\rangle$ are odd functions in z. Thus $d_{cv}^z = 0$.

1. Long-axis electric dipole matrix element

Using Eq. (2) the long-axis electric dipole matrix element can be written

$$d_{cv}^x(k) = -e\frac{\langle ck|(\mathcal{H}x - x\mathcal{H})|vk\rangle}{E_c(k) - E_v(k)}$$

$$= \frac{-e}{E_{cv}(k)N} \sum_{n,p,m,q} c_q^*(k) v_p(k) e^{ik(n-m)l} \times \langle mq|(\mathcal{H}x - x\mathcal{H})|np\rangle, \tag{5}$$

where $E_{cv} = E_c - E_v$. The matrix element $\langle mq|x\mathcal{H}|np\rangle$ is found by inserting the completeness relation $\Sigma_{n,p}|np\rangle\langle np| = 1$ between x and $\mathcal{H}$ and using the fact that for x_{mq} being the x coordinate of atom (m,q), one has

$$\langle mq|x - \frac{x_{mq} + x_{m'q'}}{2}|m'q'\rangle = 0$$

due to symmetry and thus

$$\langle mq|x\mathcal{H}|np\rangle = \sum_{m',q'} \langle mq|x|m'q'\rangle\langle m'q'|\mathcal{H}|np\rangle$$

$$= \sum_{m',q'} \frac{x_{mq} + x_{m'q'}}{2}\langle mq|m'q'\rangle\langle m'q'|\mathcal{H}|np\rangle$$

$$= x_{mq}\langle mq|\mathcal{H}|np\rangle, \tag{6a}$$

$$\langle mq|\mathcal{H}x|np\rangle = x_{np}\langle mq|\mathcal{H}|np\rangle. \tag{6b}$$

Inserting Eqs. (6) into Eq. (5) one obtains

$$d_{cv}^x(k) = \frac{-e}{E_{cv}(k)N} \sum_{n,p,m,q} c_q^*(k) v_p(k) e^{ik(n-m)l} \times (x_{np} - x_{mq})\langle mq|\mathcal{H}|np\rangle$$

$$= \frac{-e}{E_{cv}(k)} \sum_{n,p,q} c_q^*(k) v_p(k) e^{iknl} \times (x_{np} - x_{0q})\langle 0q|\mathcal{H}|np\rangle, \tag{7}$$

where it has been used that in the periodic boundary condition regime, all N unit cells are identical.

2. Short-axis electric dipole matrix element

$d_{cv}^y(k)$ is obtained by replacing x with y in Eq. (7).

C. Linear Susceptibility

Since $d_{cv}^z = 0$ in our model, the linear susceptibility tensor is given by

$$\overleftrightarrow{\chi}(\omega) = \begin{bmatrix} \chi_{xx} & \chi_{xy} & 0 \\ \chi_{yx} & \chi_{yy} & 0 \\ 0 & 0 & 0 \end{bmatrix}, \tag{8}$$

where, for this case of real electric dipole matrix elements, the components are given by

$$\chi_{ab}(\omega) = \frac{2}{\pi\varepsilon_0 A} \sum_{c,v} \int_{-\pi/l}^{\pi/l} d_{cv}^a(k) d_{cv}^b(k) \frac{E_{cv}(k)dk}{E_{cv}^2(k) - \hbar^2\Omega^2}, \tag{9}$$

where ε_0 is the vacuum permittivity and A is the cross-sectional area of the polymer. The complex frequency $\Omega = \omega + i\gamma$ contains the photon frequency ω and the damping parameter γ.

III. *trans*-POLYACETYLENE

Acetylene, C_2H_2, can polymerize as *cis*- or *trans*-polyacetylene with *trans*-polyacetylene being the thermodynamically most stable configuration[8] and the focus of this paper. The *trans*-polyacetylene (PA) chain is shown in Fig. 1 with the bond lengths obtained from Ref. 14.

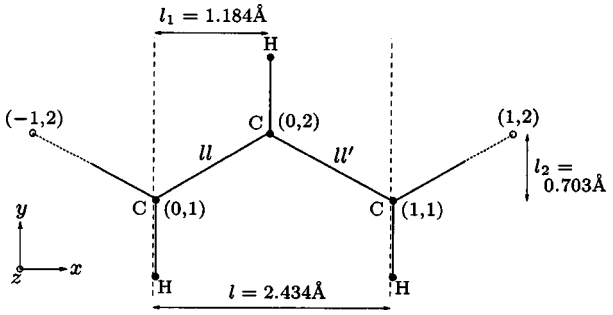

FIG. 1. The *trans*-polyacetylene chain. The coordinates (n,p) indicate carbon atom p in the nth unit cell. The bonding lengths are $ll=1.377$ Å and $ll'=1.434$ Å.

A. Band structure

For *trans*-polyacetylene Eq. (3) corresponds to the following matrix eigenvalue problem:

$$\begin{bmatrix} -E(k) & e^{-ikl}\beta'+\beta \\ \beta+e^{ikl}\beta' & -E(k) \end{bmatrix}\begin{pmatrix} r_1(k) \\ r_2(k) \end{pmatrix}=\begin{pmatrix} 0 \\ 0 \end{pmatrix}, \tag{10}$$

where β and β' are the Hamilton matrix elements along ll and ll', respectively, and where the energy of a carbon $2p_z$ orbital is chosen as the zero point of the energy ($\langle np|\mathcal{H}|np\rangle\equiv 0$). Nontrivial solutions to Eq. (10) are found for

$$\begin{vmatrix} -E(k) & e^{-ikl}\beta'+\beta \\ \beta+e^{ikl}\beta' & -E(k) \end{vmatrix}=0, \tag{11}$$

corresponding to

$$E_c(k)=+\sqrt{\beta^2+\beta'^2+2\beta\beta'\cos(kl)}, \tag{12a}$$

$$E_v(k)=-\sqrt{\beta^2+\beta'^2+2\beta\beta'\cos(kl)}. \tag{12b}$$

The π-electron band structure is shown in Fig. 2. Inserting

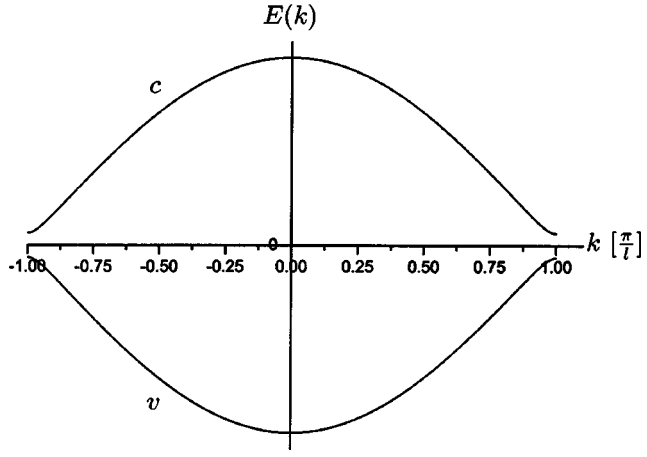

FIG. 2. The π-electron band structure of *trans*-polyacetylene.

$E_c(k)$ and $E_v(k)$ into Eq. (10) and solving for the eigenvector $\vec{r}(k)$ one obtains

$$\vec{c}(k)=\begin{pmatrix} \frac{1}{\sqrt{2}} \\ \frac{W}{\sqrt{2}} \end{pmatrix}, \quad \vec{v}(k)=\begin{pmatrix} \frac{1}{\sqrt{2}} \\ -\frac{W}{\sqrt{2}} \end{pmatrix}, \quad W=\frac{E_c}{e^{-ikl}\beta'+\beta}. \tag{13}$$

B. Electric dipole matrix element

1. Long-axis electric dipole matrix element

Inserting Eq. (13) into Eq. (7), summing over nearest neighbors, and making the approximation $l_1=l/2$ yields

$$\begin{aligned} d_{cv}^x(k)&=\frac{-e}{E_{cv}(k)}\sum_{n,p,q} c_q^*(k)v_p(k)e^{iknl}[nl+(p-q)l_1] \\ &\quad\times\langle 0q|\mathcal{H}|np\rangle \\ &=\frac{-e}{E_{cv}(k)}\frac{1}{2}[(l-l_1)\beta'(e^{ikl}W^*+e^{-ikl}W) \\ &\quad -l_1\beta(W^*+W)] \\ &=\frac{-2e}{E_{cv}^2(k)}[(l-l_1)\beta'^2-l_1\beta^2+(l-2l_1)\beta'\beta\cos(kl)] \\ &\simeq\frac{-el}{E_{cv}^2(k)}(\beta'^2-\beta^2). \end{aligned} \tag{14}$$

In connection with Eq. (14) it should be noted that *trans*-polyacetylene is degenerate in the sense that Fig. 1 might just as well have been flipped 180° about the y axis. This would lead to the transformations $\beta\rightarrow\beta'$ and thus to a change of sign in Eq. (14).

Introducing the band gap

$$E_g=E_{cv}\left(\frac{\pi}{l}\right)=2|\beta-\beta'| \tag{15}$$

and the π-band width

$$E_0=E_{cv}(0)=2|\beta+\beta'|, \tag{16}$$

Eq. (14) yields

$$d_{cv}^x(k)=\frac{elE_gE_0}{4E_{cv}^2(k)}. \tag{17}$$

A plot of $|d_{cv}^x(k)|^2$ is shown in Fig. 3.

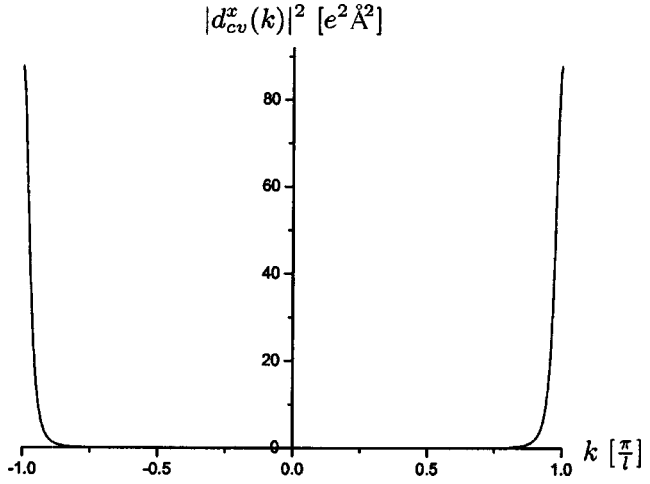

FIG. 3. The absolute square of the long-axis electric dipole matrix element of *trans*-polyacetylene.

2. Short-axis electric dipole matrix element

One obtains

$$d^y_{cv}(k) = \frac{-e}{E_{cv}(k)} \sum_{n,p,q} c^*_q(k) v_p(k) e^{iknl[(p-q)l_2]} \times \langle 0q|\mathcal{H}|np\rangle = \frac{2el_2}{E^2_{cv}(k)}[\beta'^2 + \beta^2 + 2\beta'\beta\cos(kl)] = \frac{el_2}{2}. \tag{18}$$

C. Linear susceptibility

1. Long-axis linear susceptibility

Inserting Eq. (17) into Eq. (9) one has

$$\chi_{xx,PA}(\omega) = \frac{l^2 e^2 E_g^2 E_0^2}{4\pi\varepsilon_0 A} \int_0^{\pi/l} \frac{1}{E^3_{cv}(k)} \left(\frac{1}{E^2_{cv}(k) - \hbar^2\Omega^2} \right) dk. \tag{19}$$

Since

$$\frac{dk}{dE_{cv}} = -\frac{2}{l} \frac{E_{cv}}{\sqrt{(8\beta\beta')^2 - (E^2_{cv} - 4\beta^2 - 4\beta'^2)^2}} = -\frac{2}{l} \frac{E_{cv}}{\sqrt{(E^2_{cv} - E^2_g)(E^2_0 - E^2_{cv})}}, \tag{20}$$

Eq. (19) can be written as the following integral over E_{cv}:

$$\chi_{xx,PA}(\omega) = \frac{le^2 E_g^2 E_0^2}{2\pi\varepsilon_0 A} \int_{E_g}^{E_0} \frac{1}{E^2_{cv}(E^2_{cv} - \hbar^2\Omega^2)} \times \frac{dE_{cv}}{\sqrt{(E^2_{cv} - E^2_g)(E^2_0 - E^2_{cv})}}. \tag{21}$$

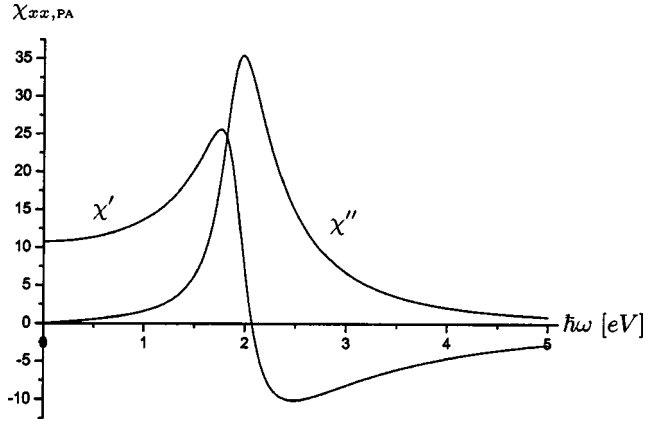

FIG. 4. The real part χ' and imaginary part χ'' of the long-axis linear susceptibility of *trans*-polyacetylene for $E_g = 1.9$ eV, $E_0 = 12.8$ eV, $\hbar\gamma = 0.2$ eV, and $A = 15.5$ Å^2.

Evaluating Eq. (21) as shown in the Appendix, one obtains the following result for the long-axis linear susceptibility of *trans*-polyacetylene:

$$\chi_{xx,PA}(\omega) = \frac{le^2}{2\pi\varepsilon_0 A} \frac{E_0^2}{E_g\hbar^2\Omega^2} \left[\frac{E_g^2}{E_g^2 - \hbar^2\Omega^2} \times \Pi\left(\frac{E_g^2 - E_0^2}{E_g^2 - \hbar^2\Omega^2}, \frac{E_g^2 - E_0^2}{E_g^2} \right) - \Pi\left(\frac{E_g^2 - E_0^2}{E_g^2}, \frac{E_g^2 - E_0^2}{E_g^2} \right) \right], \tag{22}$$

where $\Pi(n,k)$ is the complete elliptic integral of the third kind. We have adopted the MATHEMATICA definition of elliptic integrals (see the Appendix), which covers complex arguments, and we have used MATHEMATICA to evaluate the expressions. It has been verified by numerical integration that Eqs. (22) and (21) are in agreement.

The result of Eq. (22) is the equivalent of Eq. (4.4) in Ref. 16 with the present result generalized to include damping, however.

Plots in the vicinity of the band gap of the real part $\chi'_{xx,PA}(\omega)$ and imaginary part $\chi''_{xx,PA}(\omega)$ of Eq. (22) are shown in Fig. 4. The band gap E_g and the π-band width E_0 are set to their experimental values[13] $E_g = 1.9$ eV and $E_0 = 12.8$ eV corresponding to $\beta = -3.7$ eV and $\beta' = -2.7$ eV. The damping parameter γ is by fit to the experimental curves of Ref. 13 chosen as $\hbar\gamma = 0.2$ eV. According to Ref. 8 the cross sectional area of *trans*-polyacetylene is $A = 15.5$ Å^2. In addition to the shown resonance around the band gap E_g there is a weak resonance around E_0 also.

Approximate susceptibility expression. For $\hbar\omega \ll E_0$, Eq. (21) can be approximated as

$$\chi_{xx,PA}(\omega) \simeq \frac{le^2 E_g^2 E_0}{2\pi\varepsilon_0 A} \int_{E_g}^{\infty} \frac{1}{E^2_{cv}(E^2_{cv} - \hbar^2\Omega^2)} \frac{dE_{cv}}{\sqrt{E^2_{cv} - E^2_g}}, \tag{23}$$

leading to

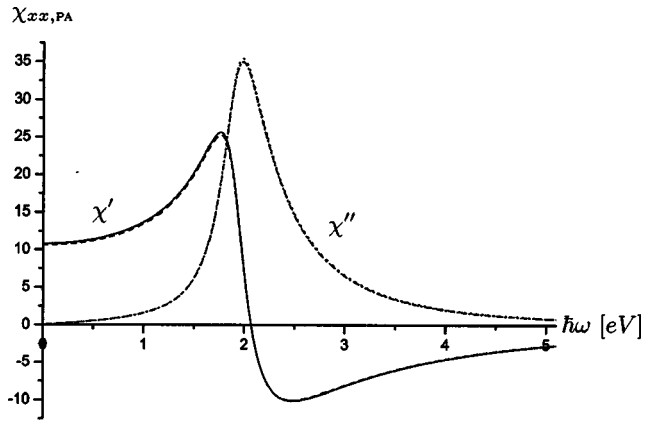

FIG. 5. A comparison of Eqs. (24) and (22) with parameters as in Fig. 4.

$$\chi_{xx,PA}(\omega)\simeq\frac{le^2E_0E_g^2}{2\pi\varepsilon_0A\hbar^2\Omega^2}\left[\frac{\arcsin\left(\frac{\hbar\Omega}{E_g}\right)}{\hbar\Omega\sqrt{E_g^2-\hbar^2\Omega^2}}-\frac{1}{E_g^2}\right]. \tag{24}$$

As an evaluation of this approximation, Fig. 5 shows a plot of Eq. (24) together with a plot of Eq. (22). The approximation is seen to be excellent in the vicinity of the band gap.

Notice that comparison of Eqs. (22) and (24) yields

$$\Pi\left(\frac{E_g^2-E_0^2}{E_g^2-\hbar^2\Omega^2},\frac{E_g^2-E_0^2}{E_g^2}\right)\simeq\frac{E_g}{E_0}\frac{\sqrt{E_g^2-\hbar^2\Omega^2}}{\hbar\Omega}\arcsin\left(\frac{\hbar\Omega}{E_g}\right),$$

$$\hbar\omega\ll E_0, \tag{25a}$$

$$\Pi\left(\frac{E_g^2-E_0^2}{E_g^2},\frac{E_g^2-E_0^2}{E_g^2}\right)\simeq\frac{E_g}{E_0}. \tag{25b}$$

Effective mass approximation. In the effective mass approximation (EMA) the band structure is given by the following parabolic expansion in the vicinity of the band gap:

$$E_{cv}(k)=E_g+\frac{\hbar^2k'^2}{2\mu},\quad k'=k-\frac{\pi}{l}, \tag{26}$$

where μ is the reduced mass given by

$$\mu\equiv\frac{\hbar^2}{\frac{d^2E_{cv}(k)}{dk^2}|_{k=\pi/l}}=4\frac{\hbar^2}{l^2}\frac{E_g}{E_0^2-E_g^2}\simeq0.06m_0, \tag{27}$$

where $m_0=9.109\times10^{-31}$ kg is the electron rest mass.

Writing the electric dipole matrix element in terms of the momentum matrix element $p_{cv}^x(k)$ one has

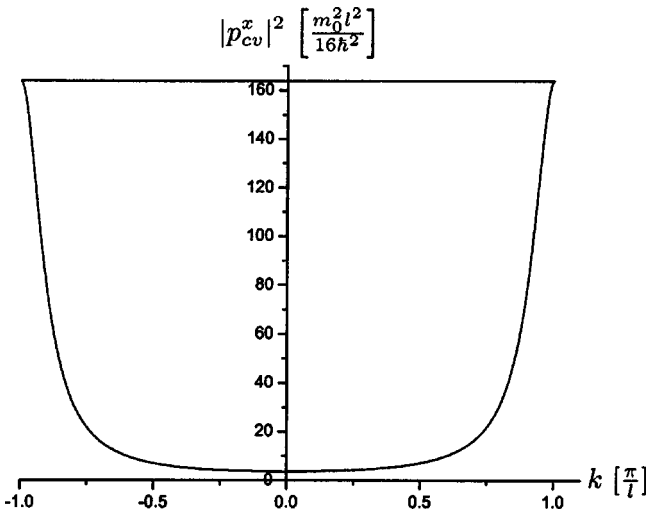

FIG. 6. The absolute square of the long-axis momentum matrix element of *trans*-polyacetylene together with the constant used in the CMMEA.

$$\begin{aligned}d_{cv}^x(k)&=\frac{-e}{E_{cv}(k)}\langle ck|(\mathcal{H}x-x\mathcal{H})|vk\rangle\\&=\frac{e\hbar^2}{2m_0E_{cv}(k)}\langle ck|\left(\frac{\partial^2}{\partial x^2}x-x\frac{\partial^2}{\partial x^2}\right)|vk\rangle\\&=\frac{-ie\hbar}{m_0E_{cv}(k)}\langle ck|\frac{\hbar}{i}\frac{\partial}{\partial x}|vk\rangle=\frac{-ie\hbar}{m_0E_{cv}(k)}p_{cv}^x(k).\end{aligned} \tag{28}$$

In the constant-momentum matrix element approximation (CMMEA) one assumes that $p_{cv}^x(k)$ is constant and equal to its value at the band gap:

$$p_{cv}^x(k)\simeq p_{cv}^x\left(\frac{\pi}{l}\right)=\frac{im_0E_{cv}\left(\frac{\pi}{l}\right)}{e\hbar}d_{cv}^x\left(\frac{\pi}{l}\right)=i\frac{m_0l}{4\hbar}E_0. \tag{29}$$

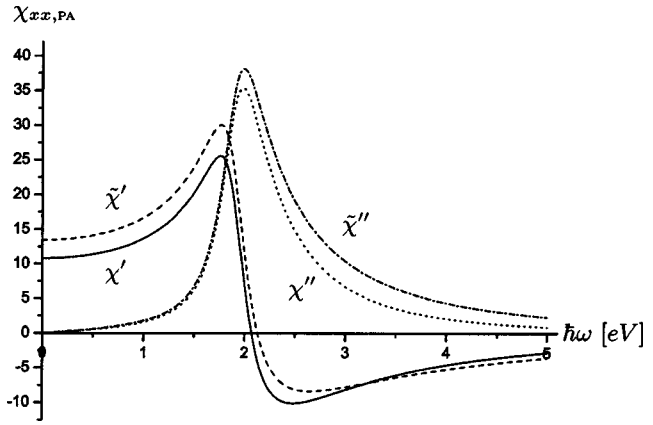

FIG. 7. The CMMEA $\tilde{\chi}$ together with the ordinary linear susceptibility χ of *trans*-polyacetylene for $Eg=1.9$ eV, $E_0=12.8$ eV, $\hbar\gamma=0.2$ eV, and $A=15.5$ Å^2.

From Fig. 6, which shows a plot of $|p^x_{cv}(k)|^2$ together with $|p^x_{cv}(\pi/l)|^2$, it can be seen that the CMMEA is significant in this case.

As shown in the Appendix the CMMEA linear susceptibility $\tilde{\chi}_{xx,PA}(\omega)$ is obtained as

$$\tilde{\chi}_{xx,PA}(\omega) = \frac{e^2 l^2 \sqrt{2\mu}}{16\hbar\varepsilon_0 A}\frac{E_0^2}{\hbar^2\Omega^2}\left[\frac{1}{\sqrt{E_g+\hbar\Omega}}+\frac{1}{\sqrt{E_g-\hbar\Omega}}-\frac{2}{\sqrt{E_g}}\right], \tag{30}$$

in agreement with Ref. 24.

Figure 7 shows a plot of the CMMEA linear susceptibility $\tilde{\chi}_{xx,PA}(\omega)$ together with $\chi_{xx,PA}(\omega)$. Inspection of Fig. 7 shows that $\chi_{xx,PA}(\omega)$ approaches zero faster than $\tilde{\chi}_{xx,PA}(\omega)$. This is due to the fact that in the CMMEA, the factor $1/E^2_{cv}(k)\sim 1/\hbar^2\omega^2$ in the electric dipole matrix element is treated as a constant. At $\hbar\omega=2.9$ eV, e.g., the CMMEA-induced error is close to 50%.

Zero-band-gap limit. The polyacetylene chain is distorted in the sense that $ll\neq ll'$ and correspondingly $\beta\neq\beta'$. As can be seen from Eq. (15), this distortion causes the introduction of a band gap E_g in the band structure, making *trans*-polyacetylene a semiconductor. This section treats the more or less hypothetical case of an undistorted and thus metallic *trans*-polyacetylene chain.

In the limit $E_g\to 0$, Eq. (22) yields

$$\begin{aligned}\lim_{E_g\to 0}\chi_{xx,PA}(\omega) &= \frac{le^2}{2\pi\varepsilon_0 A}\frac{E_0^2}{\hbar^2\Omega^2}\lim_{E_g\to 0}\left[\int_0^1 \frac{-\frac{E_g}{\hbar^2\Omega^2}dx}{\left(1-\frac{E_0^2}{\hbar^2\Omega^2}x^2\right)\sqrt{(1-x^2)\left(1+\frac{E_0^2}{E_g^2}x^2\right)}}-\int_0^1\frac{\frac{1}{E_g}dx}{\left(1+\frac{E_0^2}{E_g^2}x^2\right)^{3/2}\sqrt{1-x^2}}\right]\\ &= \frac{le^2}{2\pi\varepsilon_0 A}\frac{E_0^2}{\hbar^2\Omega^2}\lim_{E_g\to 0}\left[\frac{-E_0}{2\hbar^2\Omega^2}\int_{-1}^1\frac{\frac{E_g^2}{E_0^2}}{\left(\frac{E_g^2}{E_0^2}+x^2\right)^{3/2}}\frac{\left(\frac{E_g^2}{E_0^2}+x^2\right)dx}{\left(1-\frac{E_0^2}{\hbar^2\Omega^2}x^2\right)\sqrt{1-x^2}}-\frac{1}{2E_0}\int_{-1}^1\frac{\frac{E_g^2}{E_0^2}}{\left(\frac{E_g^2}{E_0^2}+x^2\right)^{3/2}}\frac{dx}{\sqrt{1-x^2}}\right]\\ &= -\frac{le^2}{2\pi\varepsilon_0 A}\frac{E_0}{\hbar^2\Omega^2},\end{aligned} \tag{31}$$

since

$$\lim_{E_g\to 0}\frac{\frac{E_g^2}{E_0^2}}{\left(\frac{E_g^2}{E_0^2}+x^2\right)^{3/2}} = 2\delta(x), \tag{32}$$

where $\delta(x)$ is the Dirac delta function. A plot of the linear susceptibility of *trans*-polyacetylene in the zero-band-gap limit is shown in Fig. 8. The present result is thus well behaved in the metallic limit, which is in contrast to the CMMEA case.

At this point it may be noted that Eq. (31) is in accordance with the Drude theory of metals[25] according to which

$$\chi_{xx}(\omega) = -\frac{\rho e^2}{\varepsilon_0\Omega^2\langle m^*\rangle}, \tag{33}$$

where $\rho=2/Al$ is the π-electron density and where

$$\langle m^*\rangle = \frac{\hbar^2}{\frac{l}{2\pi}\int_{-\pi/l}^{\pi/l}\frac{d^2E_v(k)}{dk^2}dk}\quad\left[E_v=-\frac{E_0}{2}\cos\left(\frac{kl}{2}\right)\right] = \frac{4\pi\hbar^2}{E_0 l^2} \tag{34}$$

is an effective mass resulting from an average over all valence states.

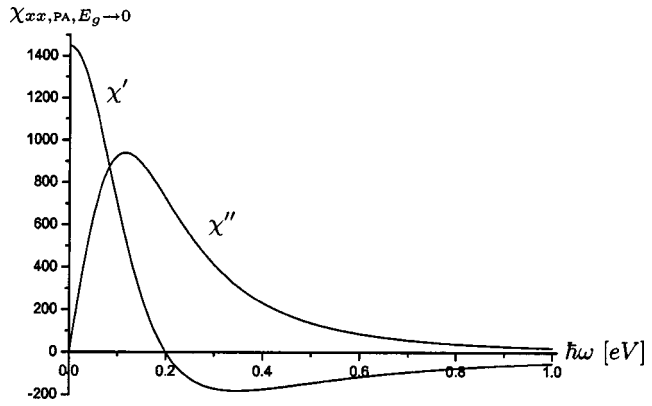

FIG. 8. The real part χ' and imaginary part χ'' of the linear susceptibility of *trans*-polyacetylene in the limit $E_g \to 0$ for $E_0 = 12.8$ eV, $\hbar\gamma = 0.2$ eV, and $A = 15.5$ Å^2.

2. Short-axis linear susceptibility

As shown in the Appendix the following result is obtained for the short-axis linear susceptibility of *trans*-polyacetylene:

$$\chi_{yy,PA}(\omega) = \frac{2l_2^2 e^2}{\pi\varepsilon_0 lA}\frac{1}{E_g}\left[\frac{\hbar^2\Omega^2}{E_g^2-\hbar^2\Omega^2} \times \Pi\left(\frac{E_g^2-E_0^2}{E_g^2-\hbar^2\Omega^2}, \frac{E_g^2-E_0^2}{E_g^2}\right) + F\left(\frac{E_g^2-E_0^2}{E_g^2}\right)\right], \tag{35}$$

where $F(k)$ is the complete elliptic integral of the first kind. A plot of $\chi_{yy,PA}(\omega)$ is shown in Fig. 9.

3. Off-diagonal linear susceptibility

One obtains

$$\chi_{xy,PA}(\omega) = \chi_{yx,PA}(\omega) = \frac{\pm l_2 e^2}{\pi\varepsilon_0 A}\frac{E_0}{E_g^2-\hbar^2\Omega^2}\Pi\left(\frac{E_g^2-E_0^2}{E_g^2-\hbar^2\Omega^2}, \frac{E_g^2-E_0^2}{E_g^2}\right), \tag{36}$$

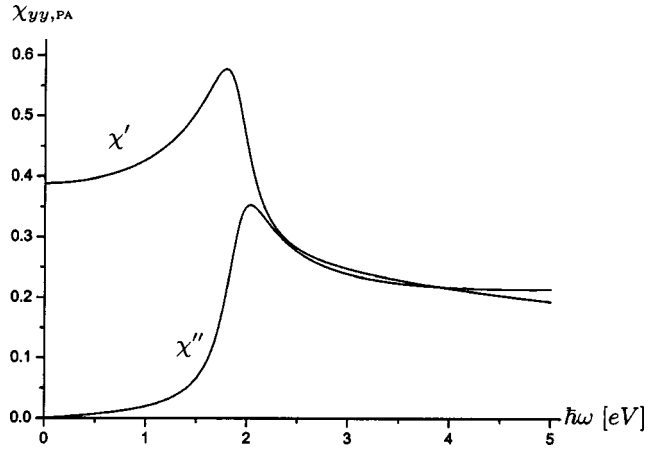

FIG. 9. The real part χ' and imaginary part χ'' of the short-axis linear susceptibility of *trans*-polyacetylene for $E_g = 1.9$ eV, $E_0 = 12.8$ eV, $\hbar\gamma = 0.2$ eV, and $A = 15.5$ Å^2.

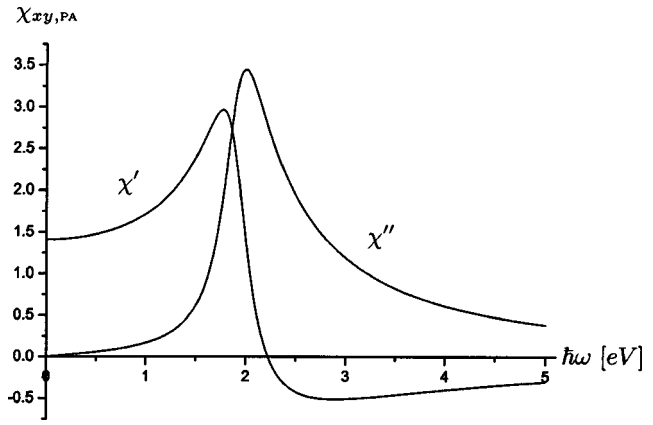

FIG. 10. The real part χ' and imaginary part χ'' of the off-diagonal linear susceptibility of *trans*-polyacetylene for $E_g = 1.9$ eV, $E_0 = 12.8$ eV, $\hbar\gamma = 0.2$ eV, and $A = 15.5$ Å^2.

where the different signs apply to the two degenerate states mentioned in the comment following Eq. (14) with the plus sign applying to the configuration of Fig. 1. A plot of $\chi_{xy,PA}(\omega)$ is shown in Fig. 10. Notice that the following relation applies[9]:

$$\chi''_{xy,PA}(\omega) = \pm\sqrt{\chi''_{xx,PA}(\omega)\chi''_{yy,PA}(\omega)}. \tag{37}$$

IV. POLY(*para*-PHENYLENE)

The poly(*para*-phenylene) (PPP) chain, $(C_6H_4)_n$, is shown in Fig. 11. The structure parameters are from Ref. 22. Note that the adjacent benzene rings in a PPP chain are twisted approximately 26° with respect to each other.[22] In the present paper, however, this torsion is disregarded, and the PPP chain is treated as a planar molecule with π orbitals coupling to other π orbitals only, since this assumption simplifies the derivations considerably.

A. Band structure

Disregarding wave function overlaps, using the same value β for all Hamilton matrix elements, and including nearest-neighbor elements only one obtains

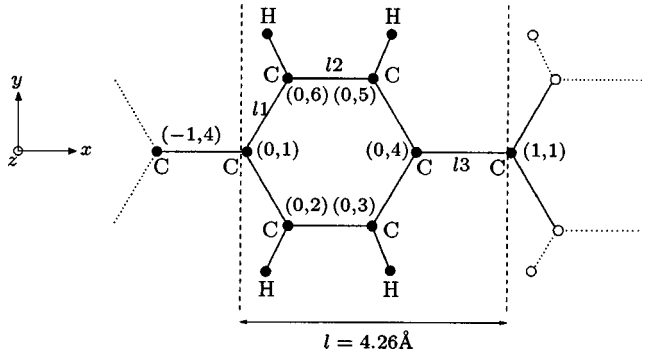

FIG. 11. The poly(*para*-phenylene) chain. The coordinates (n,p) indicate a carbon atom p in the nth unit cell. Bonding lengths are $l_1 = 1.407$ Å, $l_2 = 1.388$ Å, and $l_3 = 1.465$ Å and angles are $\angle(123) = 121°$, $\angle(612) = 118°$.

$$\begin{bmatrix} -E(k) & \beta & 0 & e^{-ikl}\beta & 0 & \beta \\ \beta & -E(k) & \beta & 0 & 0 & 0 \\ 0 & \beta & -E(k) & \beta & 0 & 0 \\ e^{ikl}\beta & 0 & \beta & -E(k) & \beta & 0 \\ 0 & 0 & 0 & \beta & -E(k) & \beta \\ \beta & 0 & 0 & 0 & \beta & -E(k) \end{bmatrix} \times \begin{pmatrix} r_1(k) \\ r_2(k) \\ r_3(k) \\ r_4(k) \\ r_5(k) \\ r_6(k) \end{pmatrix} = \begin{pmatrix} 0 \\ 0 \\ 0 \\ 0 \\ 0 \\ 0 \end{pmatrix}. \tag{38}$$

Since the xz plane is a plane of symmetry of the PPP chain, a complete set of eigenstates can be constructed consisting of functions that are of definite parity in y. The 6×6 matrix eigenvalue problem of Eq. (38) can therefore be decomposed into two smaller eigenvalue problems concerning eigenstates of either even or odd parity in y.

1. Eigenstates of even parity

In the case of eigenstates of even parity one has the unknown eigenvector components

$$r_1, \quad r_2=r_6, \quad r_3=r_5, \quad r_4, \tag{39}$$

leading to the following matrix eigenvalue problem:

$$\begin{bmatrix} -E(k) & 2\beta & 0 & e^{-ikl}\beta \\ \beta & -E(k) & \beta & 0 \\ 0 & \beta & -E(k) & \beta \\ e^{ikl}\beta & 0 & 2\beta & -E(k) \end{bmatrix} \begin{pmatrix} r_1(k) \\ r_2(k) \\ r_3(k) \\ r_4(k) \end{pmatrix} = \begin{pmatrix} 0 \\ 0 \\ 0 \\ 0 \end{pmatrix}. \tag{40}$$

Equation (40) has the following four nontrivial solutions:

$$E(k)=\pm|\beta|\sqrt{3\pm\sqrt{8}\cos\left(\frac{kl}{2}\right)}, \tag{41}$$

with corresponding eigenvectors

$$\vec{r}_e(k)=\frac{1}{2}\begin{pmatrix} \dfrac{(\varrho^2-1)e^{-ikl}+2}{\varrho^3-3\varrho} \\ \dfrac{1+e^{-ikl}}{\varrho^2-3} \\ \dfrac{\varrho^2-2+e^{-ikl}}{\varrho^3-3\varrho} \\ 1 \\ \dfrac{\varrho^2-2+e^{-ikl}}{\varrho^3-3\varrho} \\ \dfrac{1+e^{-ikl}}{\varrho^2-3} \end{pmatrix}, \tag{42}$$

where

$$\varrho=\frac{E(k)}{|\beta|}. \tag{43}$$

Equation (42) shows that

$$c_1=-v_1, \quad c_2=v_2, \quad c_3=-v_3. \tag{44}$$

2. Eigenstates of odd parity

In this case one has the eigenvector components

$$r_1=r_4=0, \quad r_2=-r_6, \quad r_3=-r_5, \tag{45}$$

and thus the following matrix eigenvalue problem:

$$\begin{bmatrix} -E(k) & \beta \\ \beta & -E(k) \end{bmatrix} \begin{pmatrix} r_2(k) \\ r_3(k) \end{pmatrix} = \begin{pmatrix} 0 \\ 0 \end{pmatrix}. \tag{46}$$

Equation (46) has the two nontrivial solutions

$$E(k)=\pm|\beta|, \tag{47}$$

with corresponding eigenvectors

$$\vec{c}_o(k)=\frac{1}{2}\begin{pmatrix} 0 \\ 1 \\ -1 \\ 0 \\ 1 \\ -1 \end{pmatrix}, \tag{48a}$$

$$\vec{v}_o(k)=\frac{1}{2}\begin{pmatrix} 0 \\ 1 \\ 1 \\ 0 \\ -1 \\ -1 \end{pmatrix}. \tag{48b}$$

The π-electron band structure is shown in Fig. 12.

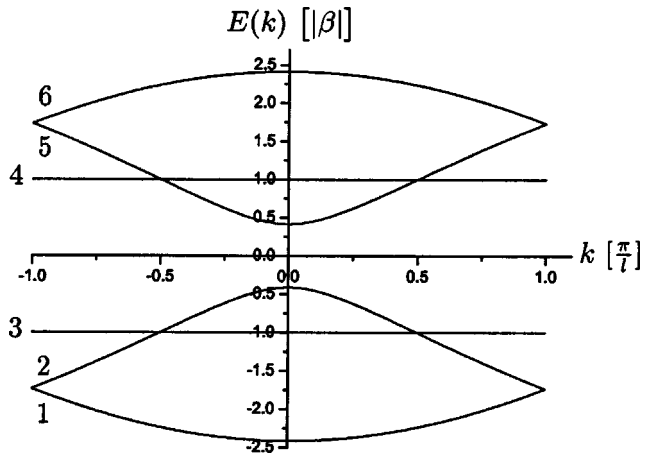

FIG. 12. The π-electron band structure of poly(*para*-phenylene) with the bands numbered from 1 to 6.

B. Electric dipole matrix element

1. Long-axis electric dipole matrix element

Making the approximation

$$\angle(123)\simeq\angle(612)\simeq 120°, \tag{49a}$$

$$l_1\simeq l_2\simeq l_3\simeq l/3=1.42\ \text{Å}, \tag{49b}$$

Eq. (7) yields

$$d^x_{cv}(k)=\frac{e|\beta|l}{3E_{cv}}\Big[c_1^*\Big(-v_4e^{-ikl}+\frac{v_2}{2}+\frac{v_6}{2}\Big)+c_2^*\Big(-\frac{v_1}{2}+v_3\Big)+c_3^*\Big(-v_2+\frac{v_4}{2}\Big)+c_4^*\Big(-\frac{v_3}{2}-\frac{v_5}{2}+v_1e^{ikl}\Big)+c_5^*\Big(-v_6+\frac{v_4}{2}\Big)+c_6^*\Big(-\frac{v_1}{2}+v_5\Big)\Big]. \tag{50}$$

Inspection of Eq. (50) shows that $d^x_{cv}(k)$ is zero for transitions between states of different parity.[27] Furthermore, a more careful inspection shows that $d^x_{cv}(k)$ is also zero for the transitions $1\rightarrow5$ and $2\rightarrow6$. The only transitions contributing to the susceptibility are thus

$$1\rightarrow6,\quad 2\rightarrow5,\quad 3\rightarrow4, \tag{51}$$

where $1\rightarrow6$ and $2\rightarrow5$ are even-even transitions and $3\rightarrow4$ is an odd-odd transition.

Even-even transitions. Using Eqs. (39) and (44) in Eq. (50) one obtains

$$d^x_{cv,ee}(k)=\frac{-e|\beta|l}{3E_{cv}}\,\frac{1+\cos(kl)}{\varrho_c^3-3\varrho_c}=\frac{-el}{24}\,\frac{\varrho_c^2-3}{\varrho_c^2},$$

$$\varrho_c=\frac{E_c(k)}{|\beta|}. \tag{52}$$

Plots of $|d^x_{61}(k)|^2$ and $|d^x_{52}(k)|^2$ are shown in Figs. 13 and 14, respectively.

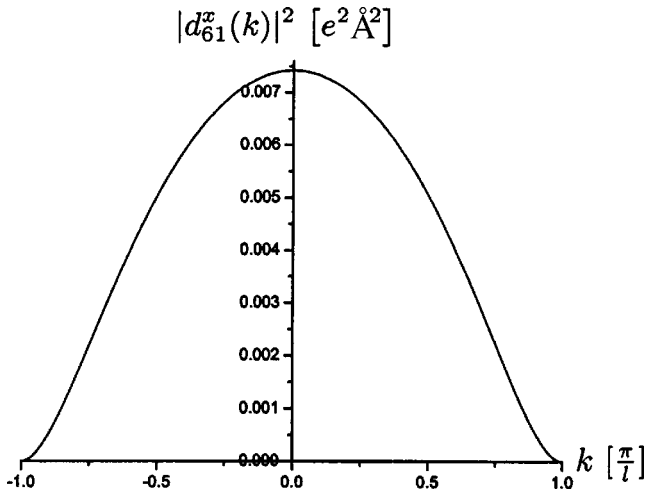

FIG. 13. The absolute square of the long-axis electric dipole matrix element of the $1\rightarrow6$ transition in poly(*para*-phenylene).

Odd-odd transitions. Using Eqs. (48) in Eq. (50) one obtains

$$d^x_{cv,oo}(k)=\frac{e|\beta|l}{3E_{cv}}=\frac{el}{6}. \tag{53}$$

2. Short-axis electric dipole matrix element

The y part of Eq. (7) yields

$$d^y_{cv}(k)=\frac{\sqrt{3}e|\beta|l}{6E_{cv}}[c_1^*(-v_2+v_6)+c_2^*(v_1)+c_3^*(v_4)+c_4^*(-v_3+v_5)+c_5^*(-v_4)+c_6^*(-v_1)], \tag{54}$$

which shows that the contributing transitions are

$$1\rightarrow4,\quad 2\rightarrow4,\quad 3\rightarrow5,\quad 3\rightarrow6, \tag{55}$$

where $1\rightarrow4$, $2\rightarrow4$ and $3\rightarrow5$, $3\rightarrow6$ are even-odd and odd-even transitions, respectively.

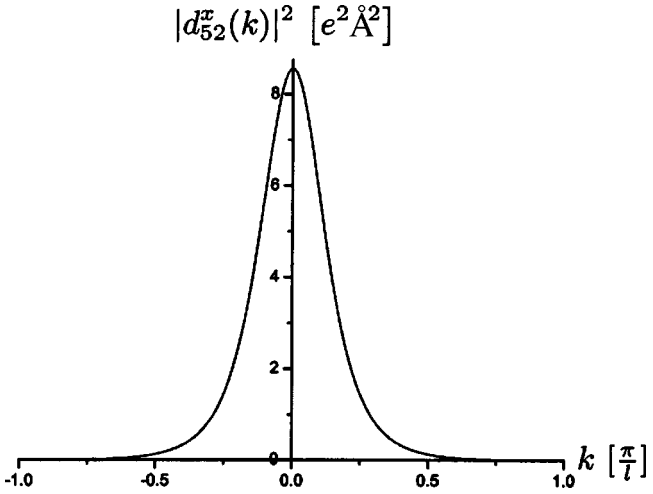

FIG. 14. The absolute square of the long-axis electric dipole matrix element of the $2\rightarrow5$ transition in poly(*para*-phenylene).

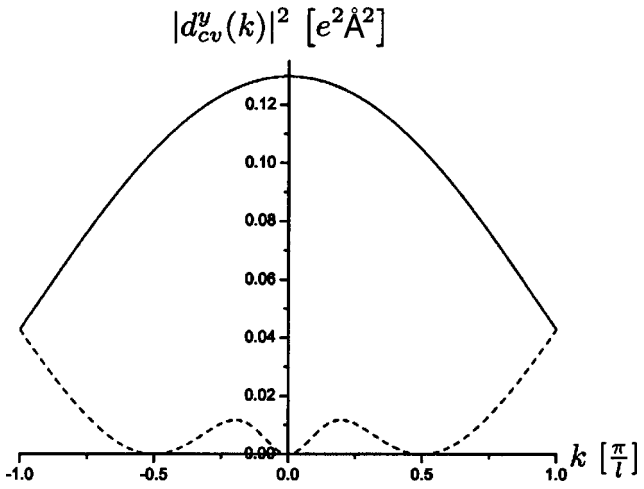

FIG. 15. The absolute square of the short-axis electric dipole matrix element of poly(*para*-phenylene). The solid line shows $|d^y_{41}(k)|^2=|d^y_{63}(k)|^2$ and the dashed line shows $|d^y_{42}(k)|^2=|d^y_{53}(k)|^2$.

Even-odd transitions. Inserting Eq. (48a) into Eq. (54) and using Eq. (42) yields

$$|d^y_{cv,oe}(k)|^2=\frac{e^2\beta^2l^2}{12E_{cv}^2}|v_1-v_4|^2$$
$$=\frac{e^2\beta^2l^2}{12E_{cv}^2}\frac{(\varrho_v+1)^2(\varrho_v^2-2\varrho_v-1)}{-8\varrho_v}$$
$$=\frac{e^2l^2}{96}\frac{(\varrho_v+1)^2(\varrho_v^2-2\varrho_v-1)}{-\varrho_v(1-\varrho_v)^2}$$
$$=\frac{e^2l^2}{96}\left[2\frac{(\varrho_v+1)^2}{\varrho_v(\varrho_v-1)^2}-\frac{(\varrho_v+1)^2}{\varrho_v}\right]. \quad (56)$$

Odd-even transitions. Inserting Eq. (48b) into Eq. (54) yields

$$|d^y_{cv,eo}(k)|^2=\frac{e^2\beta^2l^2}{12E_{cv}^2}|-c_1^*-c_4^*|^2$$
$$=\frac{e^2l^2}{96}\left[\frac{(1-\varrho_c)^2}{\varrho_c}-2\frac{(1-\varrho_c)^2}{\varrho_c(1+\varrho_c)^2}\right]. \quad (57)$$

Figure 15 shows plots of $|d^y_{cv}(k)|^2$.

C. Linear susceptibility

1. Long-axis linear susceptibility

Inserting Eqs. (52) and (53) into Eq. (9) yields

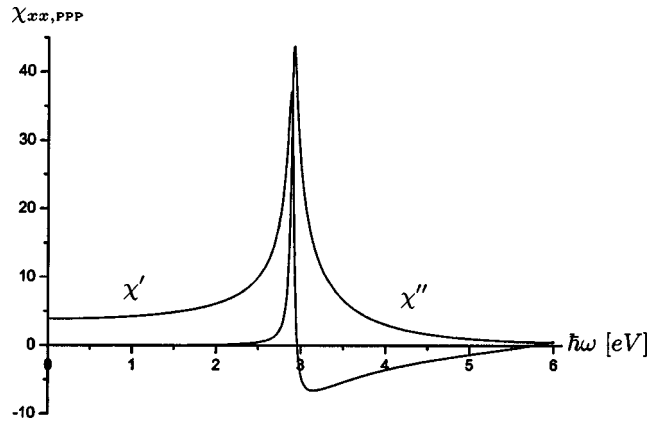

FIG. 16. The real part χ' and imaginary part χ'' of the long-axis linear susceptibility of poly(*para*-phenylene) for $E_g=2.9$ eV, $\hbar\gamma=0.03$ eV, and $A=21.5$ Å^2.

$$\chi_{xx,PPP}(\omega)=\frac{e^2|\beta|l^2}{72\pi\varepsilon_0A}\int_0^{\pi/l}\left[\left(\frac{\varrho_6^2-3}{\varrho_6^2}\right)^2\frac{\varrho_6}{4\beta^2\varrho_6^2-\hbar^2\Omega^2}+\left(\frac{\varrho_5^2-3}{\varrho_5^2}\right)^2\frac{\varrho_5}{4\beta^2\varrho_5^2-\hbar^2\Omega^2}\right]dk$$
$$+\frac{e^2l}{9\varepsilon_0A}\frac{2|\beta|}{4\beta^2-\hbar^2\Omega^2}. \quad (58)$$

Introducing the normalized band gap ϱ_g and the normalized π-band width ϱ_0

$$\varrho_g=E_g/|\beta|=2\sqrt{3-\sqrt{8}}, \quad (59a)$$
$$\varrho_0=E_0/|\beta|=2\sqrt{3+\sqrt{8}}, \quad (59b)$$

and evaluating according to the Appendix, one obtains the following for the long-axis linear susceptibility of poly(*para*-phenylene):

$$\chi_{xx,PPP}(\omega)=\frac{le^2}{4\pi\varepsilon_0A}\frac{E_0^2}{E_g\hbar^2\Omega^2}\left[\frac{\hbar^2\Omega^2}{9E_0^2}F\left(\frac{E_g^2-E_0^2}{E_g^2}\right)+\frac{\left(E_g-\frac{\hbar^2\Omega^2}{3E_0}\right)^2}{E_g^2-\hbar^2\Omega^2}\Pi\left(\frac{E_g^2-E_0^2}{E_g^2-\hbar^2\Omega^2},\frac{E_g^2-E_0^2}{E_g^2}\right)-\Pi\left(\frac{E_g^2-E_0^2}{E_g^2},\frac{E_g^2-E_0^2}{E_g^2}\right)\right]$$
$$+\frac{le^2}{9\varepsilon_0A}\frac{2|\beta|}{4\beta^2-\hbar^2\Omega^2}, \quad (60)$$

which can be approximated using Eqs. (25). Plots of $\chi'_{xx,PPP}(\omega)$ and $\chi''_{xx,PPP}(\omega)$ are shown in Fig. 16. The band gap is set to its experimental value[13] of $E_g=2.9$ eV corresponding to $\beta=-3.5$ eV and $E_0=16.9$ eV, and by a fit

to the experimental curves of Ref. 13 the damping parameter γ is chosen as $\hbar\gamma=0.03$ eV. The cross-sectional area is[21] $A=21.5$ Å^2. Comparison of Fig. 16 with Ref. 13 shows that the experimental dc susceptibility $\chi'_{xx,PPP}(0)$ is approximately 9 whereas Eq. (60) yields $\chi'_{xx,PPP}(0)\simeq 3.9$.

2. Short-axis linear susceptibility

As shown in the Appendix one obtains the following approximative expression for the imaginary part of the short-axis linear susceptibility of poly(*para*-phenylene):

$$\chi''_{yy,PPP}(\omega)\simeq\frac{e^2|\beta|l}{3\pi\varepsilon_0 A}\frac{(1-z^2)^2-2(1-z)^2}{z(1+z)}\mathrm{Im}\left\{\frac{1}{\hbar\Omega}\left[\frac{4(|\beta|-\hbar\Omega)^2}{E_g[E_g^2-4(|\beta|-\hbar\Omega)^2]}\Pi\left(\frac{E_g^2-E_0^2}{E_g^2-4(|\beta|-\hbar\Omega)^2},\frac{E_g^2-E_0^2}{E_g^2}\right)\right.\right.$$
$$-\pi\frac{|\beta|-\hbar\Omega}{\sqrt{E_0^2-4(|\beta|-\hbar\Omega)^2}\sqrt{E_g^2-4(|\beta|-\hbar\Omega)^2}}-\frac{4(|\beta|+\hbar\Omega)^2}{E_g[E_g^2-4(|\beta|+\hbar\Omega)^2]}\Pi\left(\frac{E_g^2-E_0^2}{E_g^2-4(|\beta|+\hbar\Omega)^2},\frac{E_g^2-E_0^2}{E_g^2}\right)$$
$$\left.\left.-\pi\frac{(|\beta|+\hbar\Omega)\sqrt{E_g^2+4(|\beta|+\hbar\Omega)^2}}{\sqrt{E_0^2-4(|\beta|+\hbar\Omega)^2}[E_g^2-4(|\beta|+\hbar\Omega)^2]^{3/2}}\right]\right\},$$

$$z=\begin{cases}\dfrac{\varrho_g}{2} & \text{for } \hbar\omega<|\beta|\left(1+\dfrac{\varrho_g}{2}\right),\\[2ex] \dfrac{\hbar\omega-|\beta|}{|\beta|} & \text{for } |\beta|\left(1+\dfrac{\varrho_g}{2}\right)\leqslant\hbar\omega\leqslant|\beta|\left(1+\dfrac{\varrho_0}{2}\right),\\[2ex] \dfrac{\varrho_0}{2} & \text{for } \hbar\omega>|\beta|\left(1+\dfrac{\varrho_0}{2}\right).\end{cases}\tag{61}$$

Figure 17 shows a plot of Eq. (61) together with a numerical evaluation of Eq. (A12). The approximation made in Eq. (A13) is thus seen to be reasonable. The resonance shown in Fig. 17 lies at $\hbar\omega\approx|\beta|(1+\varrho_g/2)\simeq 4.95$ eV and corresponds to the $2\rightarrow 4$ and $3\rightarrow 5$ transitions. Another resonance lies at $\hbar\omega\approx|\beta|(1+\varrho_0/2)\simeq 11.95$ eV and corresponds to the $1\rightarrow 4$ and $3\rightarrow 6$ transitions.

V. COMPARISON

A significant advantage of the analytic expressions (22) and (60) [in contrast to Eqs. (21) and (58)] is that certain similarities are readily identified. Hence, comparison of Eqs. (22) and (60) shows that the E_g and E_0 dependences of the Π function parameters are identical. Furthermore, for photon energies well below $3E_0$, the factors preceding the Π integrals are approximately identical. The differences between the two expressions are a factor of 2 and two additional terms in the PPP expression. As for the additional term containing the F integral, the preceding factor is approximately zero for $\hbar\omega\ll 3E_0$, and the odd-transition contribution is significant for photon energies in the vicinity of $2|\beta|=7$ eV only. The factor of 2 in favor of PA has the following origin. According to Eqs. (12) and (41) the cosine arguments of the PA and PPP expressions for $E(k)$ are kl and $kl/2$, respectively, giving a factor of 2 in favor of PPP in the expression for the density of states dk/dE. Furthermore, comparison of Eqs. (17) and (52) yields a factor of 4 in favor of PA in the expressions for $|d^x_{cv}|^2$:

$$d^x_{cv,PA}=\frac{el}{4}\frac{E_gE_0}{E_{cv}^2},\tag{62a}$$

$$d^x_{cv,PPP}=\frac{-el}{24}\frac{E_{cv}^2-12\beta^2}{E_{cv}^2}=\frac{-el}{24}\frac{E_{cv}^2-3E_gE_0}{E_{cv}^2}$$
$$\simeq\frac{el}{8}\frac{E_gE_0}{E_{cv}^2},\quad \hbar\omega\ll E_0.\tag{62b}$$

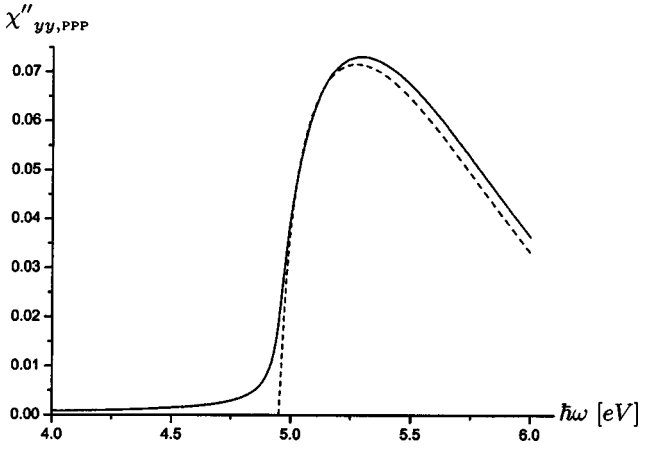

FIG. 17. The solid line shows a numerical evaluation of Eq. (A12) and the dashed line shows the approximated result of Eq. (61).

VI. SUMMARY AND CONCLUSION

In this paper we have found the linear susceptibility tensor of *trans*-polyacetylene and the long-axis linear susceptibility and the imaginary part of the short-axis linear susceptibility of poly(*para*-phenylene). Even though the structures of these two conjugated polymers are widely different, remarkably similar results have been obtained. Hence, the present work suggests that for photon energies around the band gap, the long-axis linear optical susceptibility of a general conjugated polymer can be written as

$$\chi_{xx,CP}(\omega)=K\frac{le^2}{\pi\varepsilon_0 A}\frac{E_0^2}{E_g\hbar^2\Omega^2}\left[\frac{E_g^2}{E_g^2-\hbar^2\Omega^2}\times\Pi\left(\frac{E_g^2-E_0^2}{E_g^2-\hbar^2\Omega^2},\frac{E_g^2-E_0^2}{E_g^2}\right)-\Pi\left(\frac{E_g^2-E_0^2}{E_g^2},\frac{E_g^2-E_0^2}{E_g^2}\right)\right],$$

$$\hbar\Omega=\hbar\omega+i\hbar\gamma, \tag{63}$$

where γ is the damping parameter and where E_g, E_0, A, l, and K are material-dependent constants. The band gap E_g and the π-band width E_0 characterize the band structure, the cross-sectional area A and the lattice constant l characterize the size of the unit cell, and K is given by the density of states and the size of the long-axis electric dipole matrix element.

It is hoped that the distinct way in which Eq. (63) depends on the above-mentioned parameters serves to clarify the influence of these parameters on the optical properties of conjugated polymers.

In our future work we intend to generalize the present results to include excitonic and polaronic effects. This is expected to result in a substantial improvement of the model.

ACKNOWLEDGMENTS

Financial support from the Danish Technical Science Council STVF, talent Grant No. 56-00-0290, is gratefully acknowledged.

APPENDIX

Long-axis linear susceptibility of polyacetylene

Introducing the shorthand notation

$$a^2=E_0^2-E_g^2, \tag{A1a}$$

$$x^2=\frac{E_{cv}^2-E_g^2}{E_0^2-E_g^2}, \tag{A1b}$$

$$S=\frac{le^2E_0^2E_g^2}{2\pi\varepsilon_0 A}, \tag{A1c}$$

one has the following for Eq. (21):

$$\begin{aligned}\chi_{xx,PA}(\omega)&=S\int_0^1\frac{1}{a^2x^2+E_g^2}\frac{1}{a^2x^2+E_g^2-\hbar^2\Omega^2}\frac{1}{\sqrt{a^2x^2(a^2-a^2x^2)}}\times\frac{a^2x}{\sqrt{E_g^2+a^2x^2}}dx\\&=S\int_0^1\frac{1}{a^2x^2+E_g^2}\frac{1}{a^2x^2+E_g^2-\hbar^2\Omega^2}\times\frac{dx}{\sqrt{(1-x^2)(E_g^2+a^2x^2)}}\\&=\frac{S}{E_g}\int_0^1\left(\frac{1}{\frac{E_g^2\hbar^2\Omega^2-\hbar^4\Omega^4}{1+\frac{a^2}{E_g^2-\hbar^2\Omega^2}x^2}}-\frac{1}{\frac{E_g^2\hbar^2\Omega^2}{1+\frac{a^2}{E_g^2}x^2}}\right)\times\frac{1}{\sqrt{(1-x^2)\left(1+\frac{a^2}{E_g^2}x^2\right)}}dx.\end{aligned} \tag{A2}$$

Equation (A2) is a sum of two complete elliptic integrals of the third kind, $\Pi(n,k)$, defined by

$$\Pi(n,k)\equiv\int_0^1\frac{1}{(1-nx^2)\sqrt{(1-x^2)(1-kx^2)}}dx, \tag{A3}$$

and Eq. (A2) can thus be written

$$\chi_{xx,PA}(\omega)=\frac{S}{E_g^3\hbar^2\Omega^2-E_g\hbar^4\Omega^4}\Pi\left(-\frac{a^2}{E_g^2-\hbar^2\Omega^2},-\frac{a^2}{E_g^2}\right)-\frac{S}{E_g^3\hbar^2\Omega^2}\Pi\left(-\frac{a^2}{E_g^2},-\frac{a^2}{E_g^2}\right). \tag{A4}$$

With a and S written in full one obtains Eq. (22).

CMMEA linear susceptibility of polyacetylene

Inserting Eqs. (26), (28), and (29) into Eq. (9) one obtains

$$\tilde{\chi}_{xx}(\omega)=\frac{e^2l^2E_0^2}{4\pi\varepsilon_0 A}\int_0^\infty \frac{1}{E_g+\frac{\hbar^2k'^2}{2\mu}\left(E_g+\frac{\hbar^2k'^2}{2\mu}\right)^2-\hbar^2\Omega^2}\,dk'$$

$$=\frac{e^2l^2\sqrt{2\mu}E_0^2}{8\pi\hbar\varepsilon_0 A}\int_0^\infty \frac{1}{E_g+x}\,\frac{1}{(E_g+x)^2-\hbar^2\Omega^2}\,\frac{dx}{\sqrt{x}}\quad\left(x=\frac{\hbar^2k'^2}{2\mu}\right)$$

$$=\frac{e^2l^2\sqrt{2\mu}E_0^2}{16\pi\hbar\varepsilon_0 A\hbar^2\Omega^2}\int_0^\infty\left[\frac{1/\sqrt{x}}{x+E_g+\hbar\Omega}+\frac{1/\sqrt{x}}{x+E_g-\hbar\Omega}-\frac{2/\sqrt{x}}{x+E_g}\right]dx, \tag{A5}$$

which integrates to Eq. (30).

Short-axis linear susceptibility of polyacetylene

Inserting Eq. (18) into Eq. (9) and using the shorthand in Eqs. (A1a) and (A1b) one obtains

$$\chi_{yy,PA}(\omega)=\frac{2l_2^2e^2}{\pi\varepsilon_0 lA}\int_0^1 \frac{1}{E_g^2-\hbar^2\Omega^2+a^2x^2}\,\frac{\sqrt{E_g^2+a^2x^2}}{\sqrt{1-x^2}}\,dx$$

$$=S\int_0^1 \frac{1}{E_g^2-\hbar^2\Omega^2+a^2x^2}\,\frac{E_g^2+a^2x^2}{\sqrt{(1-x^2)(E_g^2+a^2x^2)}}\,dx\quad\left(S=\frac{2l_2^2e^2}{\pi\varepsilon_0 lA}\right)$$

$$=S\frac{E_g}{E_g^2-\hbar^2\Omega^2}\int_0^1 \frac{1}{1+\frac{a^2}{E_g^2-\hbar^2\Omega^2}x^2}\,\frac{1}{\sqrt{(1-x^2)\left(1+\frac{a^2}{E_g^2}x^2\right)}}\,dx$$

$$+\frac{S}{E_g}\int_0^1 \frac{1}{1+\frac{a^2}{E_g^2-\hbar^2\Omega^2}x^2}\,\frac{\left(1+\frac{a^2}{E_g^2-\hbar^2\Omega^2}x^2\right)-1}{\sqrt{(1-x^2)\left(1+\frac{a^2}{E_g^2}x^2\right)}}\,dx$$

$$=S\frac{E_g}{E_g^2-\hbar^2\Omega^2}\Pi\left(-\frac{a^2}{E_g^2-\hbar^2\Omega^2},-\frac{a^2}{E_g^2}\right)+\frac{S}{E_g}\left[F\left(-\frac{a^2}{E_g^2}\right)-\Pi\left(-\frac{a^2}{E_g^2-\hbar^2\Omega^2},-\frac{a^2}{E_g^2}\right)\right], \tag{A6}$$

where F is the complete elliptic integral of the first kind:

$$F(k)\equiv\int_0^1 \frac{1}{\sqrt{(1-x^2)(1-kx^2)}}\,dx. \tag{A7}$$

Writing Eq. (A6) in full one obtains Eq. (35).

Off-diagonal linear susceptibility of polyacetylene

Inserting Eqs. (17) and (18) into Eq. (9) and using Eqs. (A1a) and (A1b) one has

$$\chi_{xy,PA}(\omega)=\chi_{yx,PA}(\omega)=\frac{l_2e^2E_gE_0}{\pi\varepsilon_0 A}\int_0^1 \frac{dx}{(E_g^2-\hbar^2\Omega^2+a^2x^2)\sqrt{(1-x^2)(E_g^2+a^2x^2)}}, \tag{A8}$$

leading to Eq. (36).

Long-axis linear susceptibility of poly(para-phenylene)

Evaluation of the first two terms in Eq. (58) yields

$$\chi_{xx,ee}(\omega)=\frac{e^2|\beta|l^2}{72\pi\varepsilon_0 A}\left[\int_{\varrho_0/2}^{\sqrt{3}}\left(\frac{\varrho_6^2-3}{\varrho_6^2}\right)^2\frac{\varrho_6}{4\beta^2\varrho_6^2-\hbar^2\Omega^2}\frac{dk}{d\varrho_6}d\varrho_6+\int_{\varrho_g/2}^{\sqrt{3}}\left(\frac{\varrho_5^2-3}{\varrho_5^2}\right)^2\frac{\varrho_5}{4\beta^2\varrho_5^2-\hbar^2\Omega^2}\frac{dk}{d\varrho_5}d\varrho_5\right]$$

$$=S\left[\int_{\varrho_0/2}^{\sqrt{3}}\left(\frac{\varrho_6^2-3}{\varrho_6^2}\right)^2\frac{\varrho_6}{4\beta^2\varrho_6^2-\hbar^2\Omega^2}\frac{-\varrho_6 d\varrho_6}{\sqrt{(\varrho_0^2/4-\varrho_6^2)(-\varrho_g^2/4+\varrho_6^2)}}\right.$$

$$\left.+\int_{\varrho_g/2}^{\sqrt{3}}\left(\frac{\varrho_5^2-3}{\varrho_5^2}\right)^2\frac{\varrho_5}{4\beta^2\varrho_5^2-\hbar^2\Omega^2}\frac{\varrho_5 d\varrho_5}{\sqrt{(\varrho_0^2/4-\varrho_5^2)(-\varrho_g^2/4+\varrho_5^2)}}\right]$$

$$=4S\int_{\varrho_g/2}^{\varrho_0/2}\left(\frac{\varrho^2-3}{\varrho}\right)^2\frac{1}{4\beta^2\varrho^2-\hbar^2\Omega^2}\frac{d\varrho}{\sqrt{(\varrho_0^2-4\varrho^2)(-\varrho_g^2+4\varrho^2)}},\quad S=\frac{e^2|\beta|l}{18\pi\varepsilon_0 A}. \tag{A9}$$

Introducing

$$a^2=(\varrho_0^2-\varrho_g^2)\beta^2=E_0^2-E_g^2, \tag{A10a}$$

$$b^2=\varrho_g^2\beta^2-\hbar^2\Omega^2=E_g^2-\hbar^2\Omega^2, \tag{A10b}$$

$$x^2=\frac{4\varrho^2-\varrho_g^2}{\varrho_0^2-\varrho_g^2}, \tag{A10c}$$

one obtains

$$\chi_{xx,ee}(\omega)=64|\beta|^3 S\int_0^1\frac{(2x^2-1)^2}{(a^2x^2+E_g^2)(a^2x^2+b^2)}\frac{dx}{\sqrt{(1-x^2)(a^2x^2+E_g^2)}}$$

$$=\frac{256|\beta|^3 S}{a^4E_g}\int_0^1\left[1+\frac{\left(b^2+\frac{a^2}{2}\right)^2}{b^2(E_g^2-b^2)\left(1+\frac{a^2}{b^2}x^2\right)}+\frac{\left(E_g^2+\frac{a^2}{2}\right)^2}{E_g^2(b^2-E_g^2)\left(1+\frac{a^2}{E_g^2}x^2\right)}\right]\frac{dx}{\sqrt{(1-x^2)\left(1+\frac{a^2}{E_g^2}x^2\right)}}$$

$$=\frac{256|\beta|^3 S}{a^4E_g}\left[F\left(-\frac{a^2}{E_g^2}\right)+\frac{\left(b^2+\frac{a^2}{2}\right)^2}{b^2(E_g^2-b^2)}\Pi\left(-\frac{a^2}{b^2},-\frac{a^2}{E_g^2}\right)+\frac{\left(E_g^2+\frac{a^2}{2}\right)^2}{E_g^2(b^2-E_g^2)}\Pi\left(-\frac{a^2}{E_g^2},-\frac{a^2}{E_g^2}\right)\right]. \tag{A11}$$

Use of the relation $(E_0^2+E_g^2)/2=3E_0E_g$ and inclusion of the odd-odd contribution leads to Eq. (60).

Short-axis linear susceptibility of poly(para-phenylene)

Inserting Eqs. (56) and (57) into Eq. (9) one obtains

$$\chi_{yy,PPP}(\omega)=S\int_{\varrho_g/2}^{\varrho_0/2}\left(\frac{(1-\varrho^2)^2-2(1-\varrho)^2}{\varrho(1+\varrho)}\right)\frac{1}{\beta^2(1+\varrho)^2-\hbar^2\Omega^2\sqrt{(\varrho_0^2-4\varrho^2)(-\varrho_g^2+4\varrho^2)}}\frac{\varrho d\varrho}{},\quad S=\frac{4e^2|\beta|l}{3\pi\varepsilon_0 A}. \tag{A12}$$

In the limit of zero damping, the imaginary part of the factor $1/[\beta^2(1+\varrho)^2-\hbar^2\Omega^2]$ is proportional to a δ function with argument $\beta^2(1+\varrho)^2-\hbar^2\omega^2$. Assuming that the slowly varying part is constant during differentiation one therefore has the following for the imaginary part of Eq. (A12):

$$\chi''_{yy,PPP}\simeq S\frac{(1-z^2)^2-2(1-z)^2}{z(1+z)}\mathrm{Im}\left\{\int_{\varrho_g/2}^{\varrho_0/2}\frac{1}{\beta^2(1+\varrho)^2-\hbar^2\Omega^2}\frac{\varrho d\varrho}{\sqrt{(\varrho_0^2-4\varrho^2)(-\varrho_g^2+4\varrho^2)}}\right\},$$

$$z=\begin{cases}\dfrac{\varrho_g}{2} & \text{for } \hbar\omega<|\beta|\left(1+\dfrac{\varrho_g}{2}\right)\\ \dfrac{\hbar\omega-|\beta|}{|\beta|} & \text{for } |\beta|\left(1+\dfrac{\varrho_g}{2}\right)\leqslant\hbar\omega\leqslant|\beta|\left(1+\dfrac{\varrho_0}{2}\right)\\ \dfrac{\varrho_0}{2} & \text{for } \hbar\omega>|\beta|\left(1+\dfrac{\varrho_0}{2}\right),\end{cases} \tag{A13}$$

where Im indicates the imaginary part. Using Eqs. (A10a), (A10c), and

$$d_{\pm}=2|\beta|\pm2\hbar\Omega, \tag{A14}$$

the integral in Eq. (A13) can be written

$$\begin{aligned}\int_0^1 \frac{1}{(2|\beta|+\sqrt{a^2x^2+E_g^2})^2-4\hbar^2\Omega^2}\frac{dx}{\sqrt{1-x^2}} &= \frac{1}{4\hbar\Omega}\int_0^1\left[\frac{1}{d_-+\sqrt{a^2x^2+E_g^2}}-\frac{1}{d_++\sqrt{a^2x^2+E_g^2}}\right]\frac{dx}{\sqrt{1-x^2}}\\ &= \frac{1}{4\hbar\Omega}\left[\frac{d_-^2}{E_g(E_g^2-d_-^2)}\Pi\left(\frac{a^2}{-E_g^2+d_-^2},-\frac{a^2}{E_g^2}\right)-\frac{\pi}{2}\frac{d_-}{\sqrt{a^2+E_g^2-d_-^2}\sqrt{E_g^2-d_-^2}}\right.\\ &\quad\left.-\frac{d_+^2}{E_g(E_g^2-d_+^2)}\Pi\left(\frac{a^2}{-E_g^2+d_+^2},-\frac{a^2}{E_g^2}\right)-\frac{\pi}{2}\frac{d_+(E_g^2+d_+^2)}{\sqrt{a^2+E_g^2-d_+^2}(E_g^2-d_+^2)^{3/2}}\right].\end{aligned} \tag{A15}$$

Writing Eq. (A15) in full one obtains Eq. (61).

*Electronic address: lynge@physics.auc.dk

[1] M. Pope, Kallmann, and P. Magnante, J. Chem. Phys. **38**, 2042 (1963).
[2] C. K. Chiang, C. R. Fincher, Y. W. Park, and A. J. Heeger, Phys. Rev. Lett. **39**, 1098 (1977).
[3] R. H. Friend *et al.*, Nature (London) **397**, 121 (1999).
[4] M. Wohlgenannt, E. J. W. List, C. Zenz, G. Leising, W. Graupner, and Z. V. Vardeny, Synth. Met. **116**, 353 (2001).
[5] S. Ramasesha and I. D. L. Albert, Chem. Phys. Lett. **196**, 287 (1992).
[6] C. Cojan, G. P. Agrawal, and C. Flytzanis, Phys. Rev. B **15**, 909 (1977).
[7] C. R. Fincher, Jr., M. Ozaki, M. Tanaka, D. Peebles, L. Lauchlan, A. J. Heeger, and A. G. MacDiarmid, Phys. Rev. B **35**, 9708 (1987).
[8] K. Shimamura, F. E. Karasz, J. A. Hirsch, and J. C. W. Chien, Makromol. Chem., Rapid Commun. **2**, 473 (1981).
[9] D. Baeriswyl, G. Harbeke, H. Kiess, E. Meier, and W. Meyer, Physica **117B & 118B**, 617 (1983).
[10] T. K. Lee and S. Kivilson, Phys. Rev. B **29**, 6687 (1984).
[11] J. L. Brédas, B. Thémans, J. G. Fripiat, and J. M. André, Phys. Rev. B **29**, 6761 (1984).
[12] J. Fink and G. Leising, Phys. Rev. B **34**, 5320 (1986).
[13] J. Fink, Synth. Met. **21**, 87 (1987).
[14] E. C. Ethridge and J. L. Fry, Phys. Rev. B **53**, 3662 (1996).
[15] M. Rohlfing and S. G. Louie, Phys. Rev. Lett. **82**, 1959 (1999).
[16] C.-S. Neumann and R. von Baltz, Phys. Rev. B **35**, 9708 (1987).
[17] J. Stampfl, S. Tasch, G. Leising, and U. Scherf, Synth. Met. **71**, 2125 (1995).
[18] G. Grem, G. Leditzky, B. Ullrich, and G. Leising, Synth. Met. **51**, 383 (1992).
[19] G. Grem, G. Leditzky, B. Ullrich, and G. Leising, Adv. Mater. **4**, 36 (1992).
[20] A. W. Grice, D. D. C. Bradley, M. T. Bernius, M. Insebasekaran, W. W. Wu, and E. P. Woo, Appl. Phys. Lett. **73**, 629 (1998).
[21] C. Ambrosch-Draxl, J. A. Majewski, P. Vogl, and G. Leising, Phys. Rev. B **51**, 9668 (1995).
[22] R. B. Capaz and M. J. Caldas, J. Mol. Struct. **464**, 31 (1999).
[23] T. B. Boykin and P. Vogl, Phys. Rev. B **65**, 035202 (2001).
[24] T. G. Pedersen and T. B. Lynge, Phys. Rev. B **65**, 085201 (2002).
[25] N. W. Ashcroft and D. N. Mermin, *Solid State Physics, International Edition* (Saunders College, Philadelphia, 1976).
[26] According to Ref. 10 the correction to the suseptibility due to such overlaps is significant only for photon energies much greater than the bandgap.
[27] The dipole operator x is an even function in y, so when $\langle c|$ and $|v\rangle$ have different parity in y, $\langle c|x|v\rangle=0$.